Int. J. Heat Mass Transfer. Vol. 17, pp. 113–123. Pergamon Press 1974. Printed in Great Britain

TURBULENT STRUCTURE OF ISOTHERMAL AND NONISOTHERMAL LIQUID METAL PIPE FLOW

L. E. HOCHREITER* and ALEXANDER SESONSKE
Department of Nuclear Engineering, Purdue University, West Lafayette, Indiana 47907, U.S.A.

(*Received* 7 *June* 1973)

Abstract—The structure of fully-developed mercury pipe flow, with and without heat transfer, was studied at a Reynolds number of 50 000 using a hot-film anemometer. Traverses were made in a 1·434 in. dia, vertical, heated test section at a constant wall heat flux of 3820 Btu/hft^2.

Axial turbulent velocity fluctuation measurements in isothermal pipe flow were made with both x-sensor and single-sensor hot-film probes. The radial turbulent velocity fluctuation intensity and the turbulent shear stress were also measured with an x-sensor probe. General agreement of the velocity results with corresponding measurements made in air indicates that the mercury flow turbulent velocity structure is similar to other fluids. The production and dissipation of turbulent kinetic energy were calculated from both single sensor and x-sensor data and were found to agree closely with the air data of Laufer.

Turbulent temperature fluctuations, measured by using the hot-film anemometer as a resistance thermometer, were found to agree with the results of other measuring techniques.

The turbulent axial heat flux, $\rho c_p \overline{u'\theta'}$, and the turbulent radial heat flux, $\rho c_p \overline{u_r'\theta'}$, were also measured with both single and x-sensor hot-film probes using a modified Kovasznay method to separate temperature and velocity sensitivities. The combination of relatively poor velocity sensitivity combined with the large temperature sensitivity and superimposed axial free convection resulted in uncertain values of $\overline{u_x'\theta'}$. The measured values of $\overline{u_r'\theta'}$ were unusually large in the wall region but indicated that convective and conductive transport were nearly equal in the turbulent core region.

NOMENCLATURE

c_p, specific heat [Btu/lbm°F];
D, test section diameter [ft];
E, anemometer instantaneous voltage [V];
e', fluctuating hot-film sensor voltage [V];
k, thermal conductivity [Btu/h ft °F];
M, Kovasznay parameter defined as

$$M = \frac{e'^2}{S\theta^2} - \overline{\theta'^2} \text{ [°F}^2\text{]}$$

$\bar{P}$, average pressure [lbf/ft^2];
Pr, Prandtl number, $Pr = \nu/\alpha$;
q_w, wall heat flux [Btu/hft^2];
R_0, test section radius [ft];
r, radial position in test section [ft];
Re, Reynolds number, $Re = DU_b/\nu$;
S_u, velocity sensitivity of hot-film sensor [V s/ft];
S_θ, temperature sensitivity of hot-film sensor [V/°F];
$\overline{T}$, $\overline{T}(\eta)$, local average temperature at a point [°F];
T_w, wall temperature [°F]
T_c, centerline temperature [°F];
T^*, friction temperature, $T^* = q_w/\rho c_p U^*$;
ΔT_s, temperature difference that the hot-film sensor is operating above the ambient temperature for a given ΔR_s [°F];
$\overline{U}_i$, tensor notation for average velocity, $\overline{U}_x$ (axial), $\overline{U}$ (radial), $\overline{U}_\phi$ (azimuthal) [ft/s];
u_i', tensor notation for fluctuating velocity components, u_x' (axial), u_r' (radial), u_ϕ' (azimuthal) [ft/s];
$\sqrt{(\overline{u_x'^2})}\sqrt{(\overline{u_x'^2})}$, root-mean-square of fluctuating velocity components [ft/s];
$\overline{u_r'u_x'}$, turbulent axial–radial velocity correlation [ft^2/s^2];
$\overline{u_r'\theta'}$, radial turbulent velocity–temperature correlation [ft°F/s];
$\overline{u_x'\theta'}$, axial turbulent velocity–temperature correlation [ft°F/s];
U_b bulk velocity [ft/s];
U^*, friction velocity, $U^* = U_b\sqrt{(f/2)}$ [ft/s];
$\overline{U}_{\text{eff}}$, effective cooling velocity for hot-film sensors [ft/s];
x_i, tensor notation for radial coordinates x, r, [ft];
X, hot-film sensitivity ratio,

$$X = \frac{S_u}{S_\theta} \text{ [°F s/ft]};$$

y, distance from pipe wall [ft];
α, thermal diffusivity [ft^2/h];
ε, dissipation of turbulent kinetic energy per unit mass [ft^2/h];

* Present address: Westinghouse Nuclear Energy Systems, PWR Division, Monroeville, Pa. 15146, U.S.A.

η, dimensionless distance from wall;
θ, turbulent temperature fluctuation [°F];
$\sqrt{(\overline{\theta'^2})}$, root-mean square of turbulent temperature fluctuation [°F];
ν, kinematic viscosity [ft²/h];
ρ, density [lbm/ft³];
τ_w, wall shear stress [lbf/ft²];
$\overline{\quad}$, time average.

I. INTRODUCTION

THE TURBULENT transfer of heat to and from fluids is one of the most important modes of industrial heat transfer. This is particularly true of the liquid metal fast breeder reactor concept which requires large power densities and heat fluxes. However, the complex nature of turbulent flow results in the governing equations becoming indeterminate, thus, preventing a straight-forward analytical solution.

In most fluids, analogies can be constructed between the heat and momentum transport so that the overall heat transfer can be predicted from the knowledge of the velocity field. While these analogies do provide an overall description of the transport, the models used are not in terms of a measurable statistical quantity which characterizes the randomly fluctuating turbulent field. Most of these analogies are not suitable for liquid metals since the modes of turbulent transport of heat and momentum are no longer similar. Other semiempirical approaches for liquid metal flows have been proposed by Martinelli [1], Dwyer [2], Jenkins [3], Kropholler and Carr [4], and many others. However, these approaches require assumptions regarding eddy transport in the flowing fluid.

The objective of this research was to measure the statistical behavior of the fluctuating temperature and velocity fields using a hot-film anemometer as a step in developing a picture of the turbulent transport of both heat and momentum which would be useful in the future formulation of models.

One of the best documented cases of turbulent transport is isothermal fully-developed pipe flow. This particular flow field includes nearly all the typical behavior of a general tubulent shear flow, i.e. production of turbulence, turbulent convection, dissipation, and turbulent diffusion. Moreover, due to symmetry, the equations for this flow field are in their simplest form. This symmetry allows the maximum amount of information to be obtained with the fewest measurements.

The transport of fluid momentum in a turbulent flow is governed by the Reynolds equations which can be derived from the classical Navier–Stokes relations as shown by Hinze [5]. The Reynolds equation for fully developed, steady pipe flow is

$$\frac{\mathrm{d}}{\mathrm{d}r}\overline{(u'_x u'_r)} = -\frac{1}{\rho}\frac{\mathrm{d}\bar{P}}{\mathrm{d}x} + \nu\frac{1}{r}\frac{\mathrm{d}}{\mathrm{d}r}\left[r\frac{\mathrm{d}\bar{U}_x}{\mathrm{d}r}\right] \tag{1}$$

A similar equation can be developed for the turbulent transfer of heat for steady, fully-developed flow in a pipe

$$\frac{\partial}{\partial r}(\overline{u'_r\theta'}) = -\bar{U}_x\frac{\partial\bar{T}}{\partial x} + \alpha\frac{1}{r}\frac{\partial}{\partial r}\left[r\frac{\partial\bar{T}}{\partial r}\right]. \tag{2}$$

In addition to the turbulent heat and momentum distributions, the distribution of turbulent kinetic energy is useful for developing flow structure information. The complete derivation of the turbulent kinetic energy equation for pipe flow is found in Hinze who used an order-of-magnitude technique to identify the significant terms for different flow regions in the pipe. Using his approach, the turbulent kinetic energy equation for the turbulent core is

$$\frac{\overline{u'_x u'_r}}{2}\frac{D}{U^{*3}}\frac{\mathrm{d}\bar{U}_x}{\mathrm{d}r} + \frac{D}{2U^*}\frac{1}{r}\frac{\mathrm{d}}{\mathrm{d}r} \times \left[r\left\{u'_r\left[\frac{P}{\rho} + \frac{(u'^2_x + u'^2_r + u'^2_\phi)}{2}\right]\right\}\right] + \frac{\varepsilon D}{2U^{*3}} = 0. \tag{3}$$

The ε in equation (3) represents the dissipation of turbulent kinetic energy while the first term represents the production of turbulent energy from the mean flow. By using single and x-sensor hot-film probes, pitot tubes, and a fluid thermocouple, all terms in equations (1)–(3) can be measured. In this study all terms except the second term in equation (3) were measured.

II. EXPERIMENTAL SYSTEM

A. *Heat transfer loop*

The flow system used in this study, shown in Fig. 1, was an especially-built heat transfer loop designed to accommodate liquids to temperatures of 200°F and pressures of 300 psia. The test fluid, mercury in this study, flowed in turn through an electrically-heated test section, a circulating pump, a full-flow filter, then downward through a return section used for pressure drop measurements. The primary flow then passed through a heat exchanger where it was cooled by the secondary water flow. The secondary water was, in turn, cooled by a chilled water supply in an adjoining laboratory.

The primary system was constructed from $1\frac{1}{4}$ in. and 1 in. Schedule 10, contour-welded, type 304, stainless steel pipe joined together by 300 psia stainless steel ring joint flanges. The 132-diameter long test section had a 65-diameter entrance length for

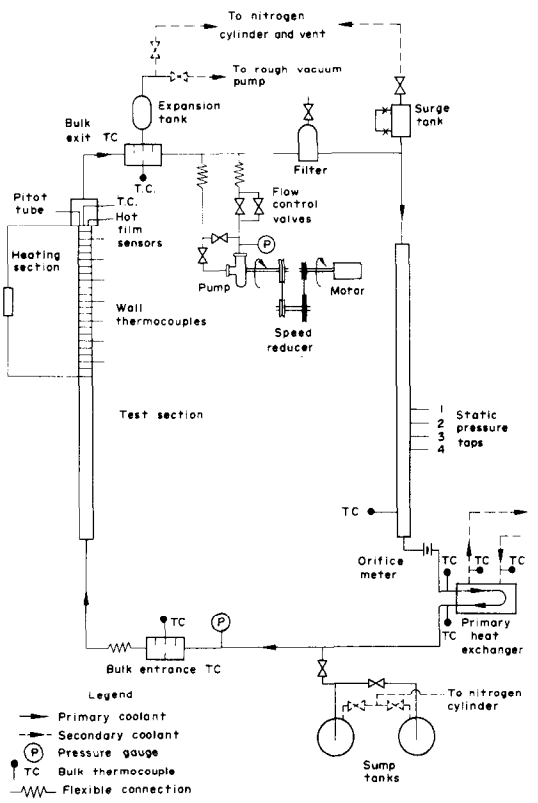

FIG. 1. Heat transfer loop.

velocity field development followed by a 67-diameter length heated with a uniform wall heat flux for thermal field development. Both the test section and return line were constructed from single pieces of contour-welded stainless steel pipe and were both preceded by straightening vanes to eliminate any swirl component in the flow due to passage through the pipe fittings. To insure both a true diameter and a smooth inside surface, both pipes were reamed and polished to a 0·7 per cent variation in the inside diameter. The inside surface was hydraulically smooth to a Reynolds number of approximately 10^6.

The traversing mechanism, located at the top of the heated test section as shown in Fig. 1, allowed three probes to be inserted into the flow 90° apart with the capability of traversing at least 75 per cent of the diameter. All three probes penetrated two pipe diameters upstream to minimize any end effects.

Test section inlet and exit temperatures were measured with thermocouples in mixing chambers which immediately preceded and followed the test section. The mercury flow rate was measured using an orifice meter and either a 60 in. (low flow rates) or a 30 in. (high flows) well-type manometer which was readable to the nearest 0·01 in. Mercury circulation was provided by a Goulds Model 3196-STD-Group M-1-1½-13 stainless steel pump whose capacity was 25 gpm at 46 ft. The filter used was a Cuno Engineering Company, Model TG1GH151802-1-SA, full-flow stainless steel filter with a 5-micron nominal, 25-micron, rating. Additional facility details are available in [6].

B. *Hot-film anemometer system*

A two-channel Thermo-Systems, Model 1050, constant-temperature hot-film anemometer system was used in this study. The system included two Model 1057 signal conditioners, zero suppression and amplifier circuits, and two Model 1040 temperature bridge switches. A Model 1040 temperature bridge switch was interconnected with each anemometer channel. When this bridge was in the velocity position, the temperature bridge circuit was bypassed and the anemometer functioned in a constant temperature mode. However, when the switch was in the temperature position, the anemometer channel functioned as an uncompensated, constant current anemometer. In this mode, a small heating current flowed through the sensor such that the hot-film sensor acted as a resistance thermometer and sensed only temperature fluctuations in the flow.

The turbulent intensities, both velocity and temperature, were measured with a Thermo-Systems, Model 1060, rms meter which had time constants adjustable up to 100 s and a frequency response down to 0·1 Hz (3 db point) at a time constant of 100 s. The instantaneous sum and difference of the two fluctuating voltage signals from the x-sensor probe were measured using a Thermo-Systems, Model 1015C, random signal correlator. Turbulent velocity and temperature fluctuations were also recorded on a four-channel Precision Instrument Company, Model 6200, FM tape recorder.

The hot-film sensors used in this study consisted of a 0·002-in. dia quartz cylinder which had a 1000-angstrom thick platinum film deposited around the outside of the cylinder. Quartz was then sputtered over the platinum film to electrically insulate it from the mercury. The active dimensions of the sensor were 0·002 in. diameter by 0·040 in. long (designated as −20 sensors by Thermo-Systems). This particular sensor size proved the most satisfactory in a trial of several sized sensors in an attempt to obtain adequate sensor velocity sensitivity with minimum sensor size. The x-sensors were standard, −20 sensors (0·002 in. dia, active length of 0·040 in.) but were inclined at 45° to the axis of the pipe.

The anemometer bridge voltage can be represented as

$$E = f(\bar{U}_{\text{eff}}, \Delta T_s) \tag{4}$$

where $\bar{U}_{\text{eff}}$ is the effective velocity for the sensor and ΔT_s is $T_s - T_a$. For a sensor placed normal to the mean flow direction, $\bar{U}_{\text{eff}} = \bar{U}_x$. By assuming that the small fluctuations in power level are due to the local turbulent velocity and temperature fluctuations, the instantaneous response equation for a sensor normal to the mean flow becomes

$$e' = S_u u'_x - S_\theta \theta' \tag{5}$$

where

$$S_u = \frac{\partial \bar{E}}{\partial \bar{U}_x} \tag{6}$$

and

$$S_\theta = \frac{\partial \bar{E}}{\partial \Delta T_s}. \tag{7}$$

The mean square of equation (5) now becomes

$$\overline{e'^2} = S_u \overline{u'^2_x} - 2S_u S_\theta \overline{u'_x \theta'} + S_\theta \overline{\theta'^2}. \tag{8}$$

Calibration curves were obtained by operating the sensor at various temperature differences in a constant temperature, low turbulent intensity flow at the pipe centerline for several different velocities. To evaluate the temperature and velocity sensitivities, the calibration results were least-squares fitted to a power law expression and then differentiated. Once the hot-film's sensitivity to both temperature and velocity fluctuations are known, equation (8) gives the relationship between the known quantities, $\overline{e'^2}$, S_u, S_θ; and the unknowns, $\overline{u'^2_x}$, $\overline{u'_x \theta}$, and $\overline{\theta'^2}$. Since there are three knowns, at least three relationships similar to equation (8) are needed to solve the problem.

The modified Kovasznay Fluctuation Diagram method suggested by Arya [7] was used to reduce the errors in calculating the desired turbulent correlations and intensities in a heated flow. In this method, an independent measurement of the turbulent temperature fluctuations was made by using the hot-film sensor as a resistance thermometer. Then letting

$$M = \frac{\overline{e'^2}}{S\theta^2} - \overline{\theta'^2}, \tag{9}$$

equation (8) becomes

$$M = X^2 \overline{u'^2_x} - 2X \overline{u'_x \theta'}. \tag{10}$$

By using the hot-wire sensor as a resistance thermometer, the intercept of the Kovasznay Diagram was then fixed at $X = 0$, and values of $\overline{u'^2_x}$ and $\overline{u'_x \theta'}$ were then calculated from the data. Unfortunately, this method did not yield the results hoped for since the hot-film sensor did not have sufficient velocity sensitivity to overcome the large temperature fluctuations and temperature sensitivity of the sensor. A similar procedure used to evaluate the x-sensor measurements in the temperature varying flow is given in [6].

III. RESULTS AND DISCUSSION

A. *Isothermal turbulent velocity fluctuation measurements*

The isothermal axial component of the turbulent velocity fluctuations, $\sqrt{(\overline{u'^2_x})}/U^*$, was measured using both a single hot-film sensor and an x-sensor probe. All data were taken at a Reynolds number of approximately 50 000 (51 000 for the single sensor data and 49 600 for the x-sensor data). The axial intensity data, measured with the single sensor and the x-sensor, are shown in Fig. 2 with the liquid data of Burchill [8] (water), Cohen [9] (water), Gardner [10] (mercury), and Patterson [11] (organic solvent); and the air data of Laufer [12] and Patel [13]. The curve shown represents data taken at different single sensor temperatures but which agreed within three per cent. Although these single sensor results are somewhat higher than most of the other work at a Reynolds number of 50 000, they are in close agreement with Patel's data taken at two larger Reynolds numbers. This trend is particularly evident near the wall region. The x-sensor axial turbulent intensity values, also shown in Fig. 2, which are approximately 10 per cent below the single sensor measurements, are in better agreement with Laufer's air data.

The radial turbulent velocity intensity, $\sqrt{(\overline{u'^2_r}/U^*)}$, calculated from the measured x-sensor data, is shown in Fig. 3 together with Burchill's Cohen's, and Laufer's data. The present results represent the average of two runs, with agreement within 11 per cent, taken at two different sensor overheats. Good agreement was obtained with Laufer's air results while Burchill's and Cohen's data are significantly higher, a difference most likely due to the sensor drift experienced during their experiments.

The present turbulent axial velocity intensity data exhibit a maximum near the wall at a y^+ value of approximately 26–33. Laufer found his axial velocity fluctuations peaked at a y^+ of approximately 20 for both his 50 000 and 500 000 Reynolds number data; Burchill found no definite peak in his axial intensity data at a Reynolds number of 50 000. Kudva's [14] axial velocity intensities, measured in ethylene glycol at a Reynolds number of 6000,

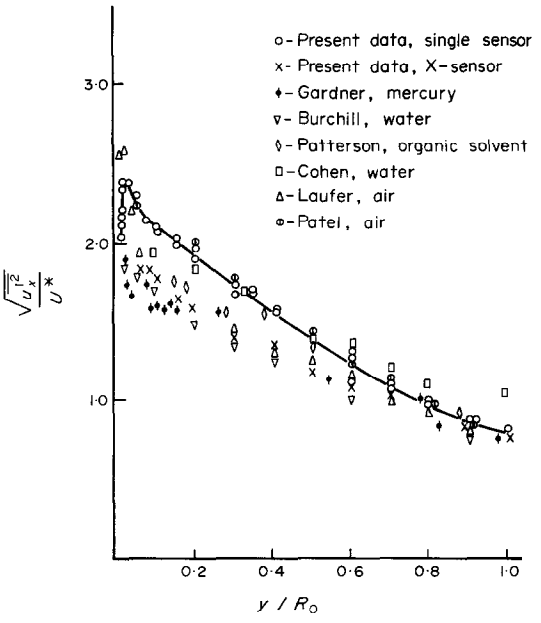

FIG. 2. Single sensor and x-sensor axial turbulent velocity fluctuations at $Re = 50000$.

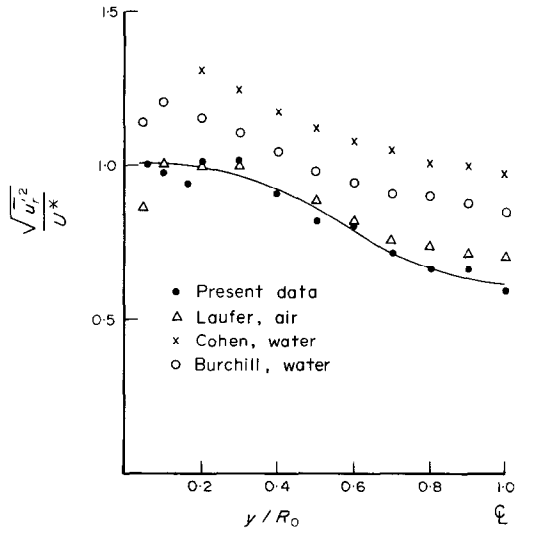

FIG. 3. X-sensor radial turbulent velocity fluctuations at $Re = 50000$.

indicated an axial intensity peak at a y^+ value of approximately 12–15. Therefore, the present data, Laufer's air measurements, and Kudva's glycol data indicate that the turbulence structure is relatively Reynolds number independent in the viscous-buffer region where $y^+ \leqslant 30$.

The location of the peak in the axial velocity intensity is significant, since it is the approximate location of the maximum production of turbulent kinetic energy. Hinze showed that the energy transfer from the mean motion, through the turbulent shear stress, only increases the axial intensity component and not the other turbulent velocity components; thus resulting in a sharp peaking of the axial intensity near the wall. The radial and aximuthal velocity fluctuation components receive energy from the axial velocity component through the pressure–velocity gradient correlation which couples the three turbulent velocity components. Since the radial velocity intensity gradient is small near the wall, it appears that the energy transfer from the axial intensity is gradual and occurs more toward the turbulent core. The energy transfer mechanism at the wall creates a large degree of anisotropy in the turbulence structure while the energy transfer among the turbulent velocity components makes the turbulence more isotropic. Therefore, the measured values of the turbulent intensity should be approximately equal at the pipe centerline. The present data indicate that the radial intensity is approximately 20 per cent smaller than the axial turbulent intensity at the pipe centerline. Laufer's air data showed that the intensities were equal thus indicating that energy transfer between the turbulent velocity components does increase the degree of isotropy.

B. *Turbulent shear stress measurements*

The turbulent shear stress was measured using two different hot-film over-heat ratios with an x-sensor. The present results are shown in Fig. 4 along with Laufer's air data and Burchill's and Cohen's water data. Also shown in Fig. 4 are plots of the total, viscous, and turbulent shear stress. The viscous shear stress was calculated from a previously measured isothermal velocity profile [6]. Present mercury results are in good agreement with both the linear total shear stress distribution and Laufer's air data. However, the water data appear to be much too low. The present measured turbulent shear stress values were larger than the predicted turbulent shear stress curve in the wall region, a tendency also observed by Laufer and Sandborn [15] in fully-developed pipe flow. In the present work, the two data points closest to the wall were corrected for velocity averaging across the sensor by using von Kármán's [16] velocity profile to calculate an average fluid velocity across the projected sensor length. The resulting velocity correction was only three per cent for the data point closest to the wall. The same correction when applied to the previously discussed radial intensity measurements yielded an even smaller effect. The present

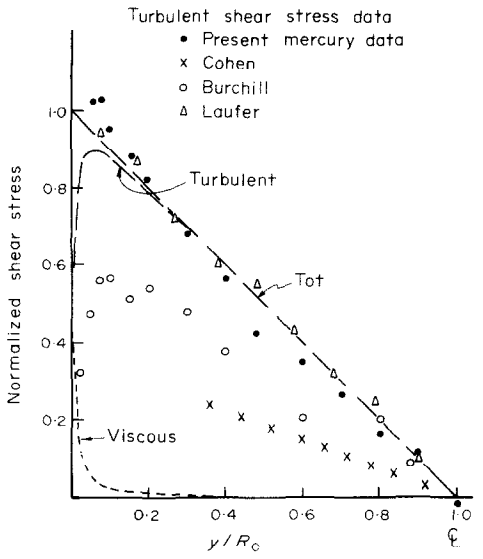

FIG. 4. Turbulent shear stress comparisons at $Re = 50000$.

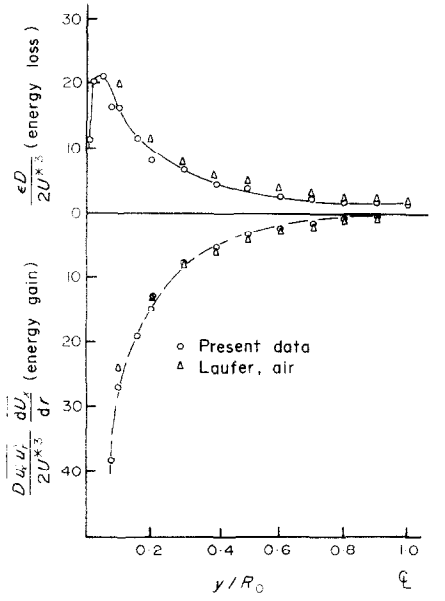

FIG. 5. Production and dissipation of turbulent kinetic energy at $Re = 50000$.

x-sensor data were also corrected for the effect of sensor yaw by using the yaw sensitivity data of Hill [17] and Schlosser [18] with the sensor response equation suggested by Hinze.

Single sensor axial turbulent velocity fluctuations were also recorded using an FM tape recorder. By applying the data analysis methods described in [6], the second moment of the spectral data was calculated to determine, ε, the dissipation of turbulent kinetic energy. Using the measured turbulent shear stress data, the mean velocity profile, and the measured pressure drop information, both the turbulent kinetic energy production and dissipation terms in equation (3) were calculated and are shown in Fig. 5. Good agreement was obtained with the turbulent production and dissipation of kinetic energy calculated from Laufer's air data at a centerline Reynolds number of 50000. Both the turbulent production and dissipation are maximum at the wall indicating that the majority of the turbulent kinetic energy which is transferred from the mean motion is dissipated immediately. The large peak in the axial turbulent intensity, shown in Fig. 2, corresponds with the approximate location of the turbulent production peak, as expected, since $\sqrt{(\overline{u_x'^2})}$ received its energy directly from the turbulent production at the wall.

C. *Turbulent temperature fluctuation measurements*

Turbulent temperature fluctuations were measured at a Reynolds number of 50000 with a constant wall heat flux of 3820 Btu/hft^2 using a standard -20 hot-film sensor as a calibrated resistance thermometer. A analysis indicated that the sensor had adequate response to 150 Hz and its 3 db point was approximately 400 Hz [6].

The measured turbulent temperature fluctuation data are shown in Fig. 6 together with the results of Hochreiter and Sesonske [19] who measured temperature fluctuations in NaK (56% K) flowing in a horizontal tube with a constant wall heat flux using a rapid response thermocouple. The data are presented as

$$\frac{\sqrt{(\overline{\theta'^2})}(T_w - T_c)}{T^{*2}}$$

in an attempt to compensate for the different physical properties of the two fluids. Normalizing the temperature fluctuations in this manner results in reasonable similarity near the centerline indicating that the hot-film sensor will give reliable values of turbulent temperature fluctuations. However, since the wall region is the location of maximum turbulent kinetic energy and temperature fluctuations, the effect of different temperature profiles will alter the temperature fluctuation production; hence, the magnitude of $\sqrt{(\overline{\theta'^2})}$. Figure 6 also indicates the large amplitude temperature fluctuations penetrate out into the turbulent core and are not confined to the wall region. Rust and Sesonske [20] and Hochreiter and Sesonske showed that the amount of penetration is a strong function of the fluid Prandtl number. Low Prandtl number fluids display a peak tempera-

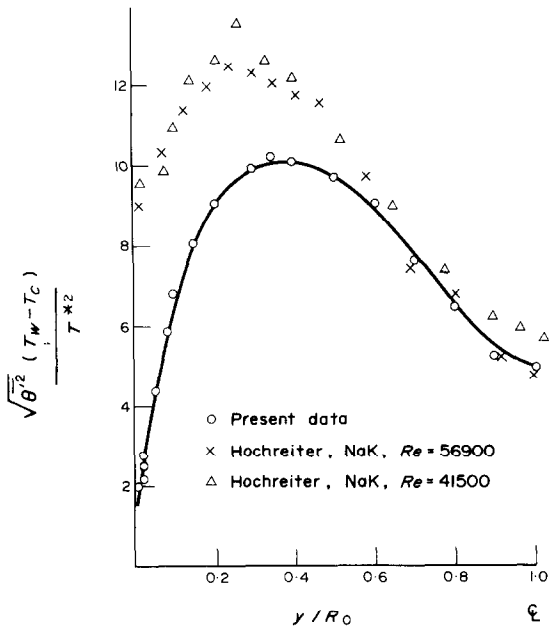

FIG. 6. Turbulent temperature fluctuations in liquid metals.

ture fluctuation at $y/R_0 = 0{\cdot}3$ while higher Prandtl number fluids exhibit temperature fluctuation peaks much closer to the wall.

D. *Turbulent axial heat flux measurements*

The turbulent axial heat flux, or the $\overline{u_x'\theta'}$ correlation, was also measured at a Reynolds number of 50000 with a wall heat flux of 3820 Btu/hft^2. The $\overline{u_x'\theta'}$ correlation was calculated using the modified Kovasznay technique described earlier.

During these experiments, it became evident that the hot-film sensor was very temperature sensitive even when operated at high overheats in the velocity mode. The large low frequency temperature fluctuations tended to overwhelm the response of the sensor to velocity fluctuations, particularly at the lower overheats. Higher sensor overheats were therefore used in an attempt to increase the velocity sensitivity. Although this mode of operation helped to some extent, the sensor's output was still strongly influenced by the large temperature fluctuations in the flow, which resulted in positive values of $\overline{u_x'\theta'}$ being calculated from equation (10).

An analysis was performed on the data to determine the likely errors in $\overline{u_x'\theta'}$ using the Kovasznay method. Since sensor calibrations were reproducible, and there was very little error in the power law fit to the calibration data; all the error in the Kovasznay method was assumed to result from fitting equation (10) with a least-squares parabola. The calculated error in the $\overline{u_x'\theta}$ data was found to be approximately 40 per cent.

The measured values of $\overline{u_x'\theta'}$ are shown in Fig. 7 along with Kudva's ethylene glycol data, Bremhorst and Bullock's [21] air data, and Burchill's water data. The mercury data are seen to be opposite in sign from the other data over most of the flow. Only

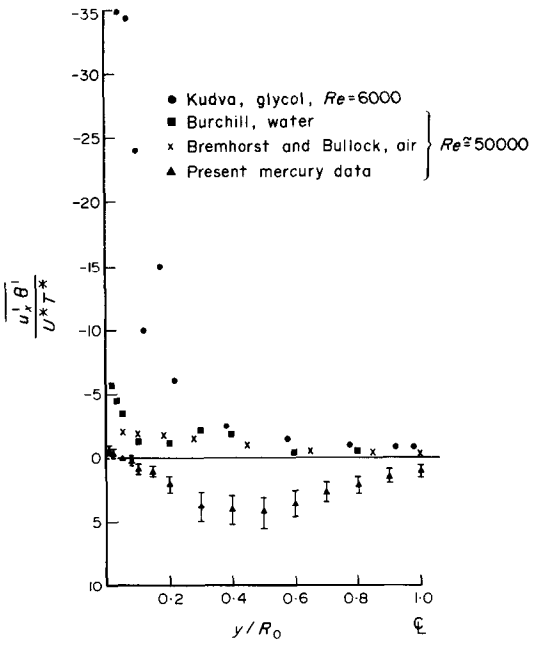

FIG. 7. Turbulent axial heat flux measurements.

at the wall, where the velocity sensitivity was relatively large and the temperature fluctuations were small, does the sign of the mercury data agree with the other data. Since the axial temperature gradient is positive, the axial turbulent velocity fluctuations will convect cooler fluid from one axial position to warmer fluid further downstream. The convection of cooler fluid into warmer fluid causes the warmer fluid to lose heat, giving rise to an expected $-\overline{u_x'\theta'}$ correlation. Arya's $\overline{u_x'\theta'}$ data for a cooled boundary layer showed a positive value which is in agreement with this simple transport approach.

Since the present $\overline{u_x'\theta'}$ results displayed the opposite sign, it was thought they were erroneous. However, recent $\overline{u_x'\theta'}$ measurements in air by Connor [22] indicate that this particular turbulent parameter is very sensitive to the amount of free convection present and will change from a negative to a positive sign before the free convection severely distorts the mean velocity field. Therefore, an attempt was made to assess the amount of free convection, if any,

in the present work. A heated velocity profile for the present conditions was calculated from the heated velocity profile measurements of Jacoby and Sesonske [23] and Horston [24]. This estimated velocity profile was much flatter at the centerline than the isothermal profile indicating that free convection was indeed present and might have caused distortion of the heated turbulent measurements. Since the accuracy of the present $\overline{u_x'\theta'}$ measurements is limited, it is not clear how significant the free convection effects are. Additional turbulent axial heat flux measurements in mercury are therefore needed over a range of wall heat flux values to resolve this picture.

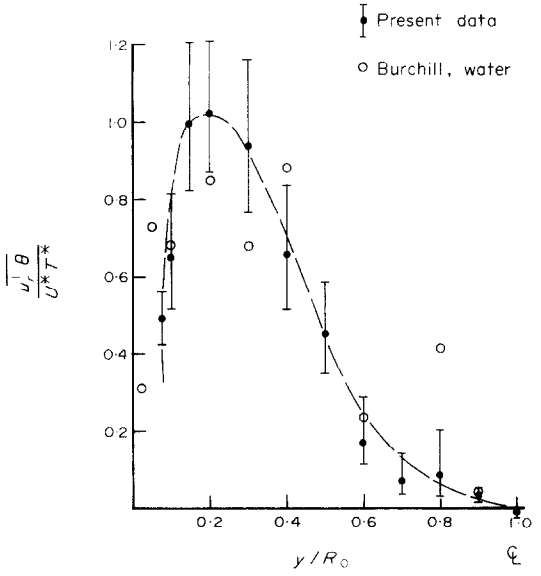

FIG. 8. Turbulent radial heat flux measurements at $Re = 50000$.

E. *Turbulent radial heat flux measurements*

The turbulent radial heat flux was also measured using an x-sensor probe at a Reynolds number of 50000 with a wall heat flux of 3820 Btu/hft^2. Response equations and calibration procedures are given in [6]. Measured values of $\overline{u_r'\theta'}$, with the calculated error, are shown in Fig. 8 with Burchill's water measurements. The present data show a consistent trend and peak at $y/R_0 = 0{\cdot}2$, while Burchill's data show no definite peak. Since radial velocity intensity in this region is nearly a constant as shown in Fig. 3, the $\overline{u_r'\theta'}$ distribution appears to be influenced more by the turbulent temperature fluctuations than by the radial velocity fluctuations.

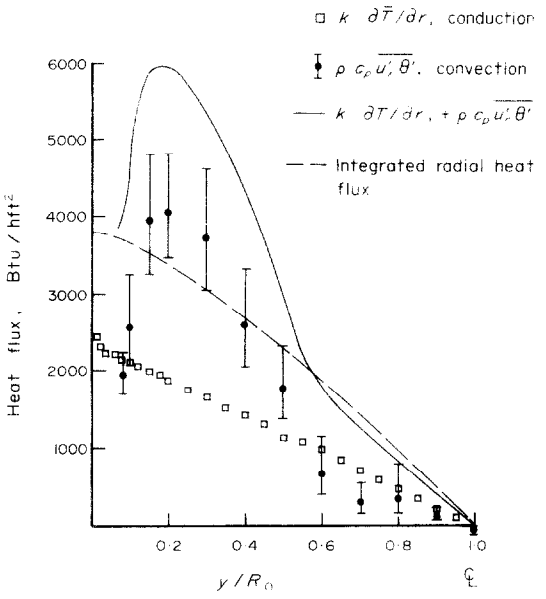

FIG. 9. Turbulent radial heat flux balance.

The magnitude of $\overline{u_r'\theta'}$ is smaller than $\overline{u_x'\theta'}$ for both the present data and Burchill's water data. Arya showed that in a nonisothermal boundary layer, the axial turbulent heat flux should be larger than the radial turbulent heat flux, $\rho c_p \overline{u_r'\theta'}$. When his analysis is applied to fully-developed pipe flow, it can be shown that the $\overline{u_r'\theta'}$ correlation is only enhanced through interaction with the mean temperature field while the $\overline{u_x'\theta'}$ correlation is "produced" by interactions with both the mean velocity and temperature fields. Therefor, $\overline{u_x'\theta'}$ is favored by the mean flow and should be larger than $\overline{u_r'\theta'}$. The present measurements and the data of both Arya and Burchill confirm this. It might also be noted that there appears to be a stronger Prandtl number effect in the $\overline{u_x'\theta'}$ data trends than in the $\overline{u_r'\theta'}$ data.

Considering an energy balance on a cylindrical shell of fluid, equation (2) can be rewritten as

$$\rho c_p \int_0^r \bar{U}(r') \frac{\partial \bar{T}}{\partial x} r' \mathrm{d}r' = r\left(\rho c_p \overline{u_r'\theta'} + k \frac{\partial \bar{T}}{\partial}\right). \tag{11}$$

By replacing the axial temperature gradient with the wall heat flux, equation (11) becomes

$$\frac{q_w}{\eta} \int_0^{\eta} \frac{\bar{U}(\eta')}{\bar{U}_b} \eta' \, \mathrm{d}\eta' = \left(\rho c_p \overline{u'\theta'} + k \frac{\partial \bar{T}}{\partial \eta}\right) \tag{12}$$

The left hand of equation (12) was calculated using Travis's [25] predicted isothermal velocity profile which was modified to account for heating. The

molecular heat flux was calculated using the slope of a previously measured temperature profile at the same conditions.

As seen from Fig. 9, the sum of the conduction and convection terms are greater than the total heat input at y/R_0 values of 0·1–0·5. Since this is physically impossible, the measured values of $\overline{u_r'\theta'}$ are apparently twice as large at $y/R_0 = 0{\cdot}2$ if the conduction flux is assumed to be correct. Since the error analysis does not explain this difference, the technique used to measure and calculate $\overline{u_r'\theta'}$ becomes suspect.

The same problems that plagued the $\overline{u_x'\theta'}$ measurements (poor velocity sensitivity, large temperature sensitivity, and very large temperature fluctuations) affected the $\overline{u_r'\theta'}$ measurements. It was hoped that by subtracting the two x-sensor signals, the temperature fluctuation and temperature sensitivity problems would be minimized. As Fig. 9 indicates, these procedures worked reasonably well in the regions of small temperature fluctuations, i.e. at the wall and centerline. However, the poorest results occurred at the location of the maximum point of the turbulent temperature fluctuations.

The data trends indicate that the convection effect was the largest at or near the maximum point of the turbulent temperature fluctuations ($y/R_0 = 0{\cdot}2$–$0{\cdot}3$). The $\overline{u_r'\theta'}$ trends also show that the conduction transport can be as large as the convection transport in the turbulent core region. The small value of $\overline{u_r'\theta'}$ at the center is due to the small production of $\overline{u_r'\theta'}$ at the center and the small $\sqrt{(\overline{u_r'^2})}$ and $\sqrt{(\overline{\theta'^2})}$ intensities in that region.

The present $\overline{u_r'\theta'}$ measurements do not appear distorted due to the superimposed free convection. The eddy diffusivity of heat predictions of Jacoby and Sesonske, as well as Horsten, indicate ε_H; therefore, $\overline{u_r'\theta'}$ should decrease as the amount of free convection increases. This trend is not observed in the present data which might indicate that the radial turbulent transport is not as seriously affected by axially-directed free convection as is the axial turbulent transport.

Figure 9 also indicates that approximately one-half the heat is transported by convection. This is consistent with the Lyon equation [26] prediction of a Nusselt number of approximately 14 for the present conditions including a molecular conduction contribution of 7·0.

Arya's air measurements in a cooled boundary layer flow show a different balance between conductive and convective heat transport. His results were also obtained using the modified Kovasznay technique. As expected in air, the heat transport by conduction was only significant at the wall with turbulent convection as the principal mode of heat transport throughout the boundary layer. The ratio of convective transport to conductive transport was approximately ten-to-one for the air boundary layer, compared with a one-to-one ratio for the present mercury pipe flow.

IV. CONCLUSIONS

The isothermal turbulent measurements show good agreement with the air data of Laufer and indicate that accurate measurements are possible with a hot-film sensor in mercury. The isothermal turbulent structure was found to be nearly the same for both air and mercury at a Reynolds number of 50000.

The heated measurements indicated different trends from other heated data and are more difficult to interpret. While the turbulent temperature fluctuations agreed with previously-measured thermocouple data, the turbulent axial heat flux measurements displayed opposite trends from similar data in other fluids. The present axial heat flux values were positive over most of the flow field and agreed with trends observed by Connor in mixed, free and forced convection in air. A close examination of other mercury data, taken in mixed convection regimes, indicated there was superimposed free convection in the present experiments which could have distorted the axial turbulent heat flux data. Therefore, additional turbulent axial heat flux measurements are needed at several wall heat flux values before final conclusions can be drawn.

The radial heat balance and radial heat flux measurements indicated that for the present Péclet number, heat is transmitted equally by the conductive and convective mechanisms near the pipe center. The turbulent radial heat flux data in the wall region appeared to be more sensitive to the turbulent temperature fluctuation field rather than the velocity fluctuation field and did not appear to be sensitive to the free convection. Both turbulent radial heat flux and temperature fluctuations exhibit a maximum in this region. The turbulent radial heat flux displayed a decrease at the wall where the conductive mechanism was the largest. The ratio of the conductive and convective transport mechanisms generally agreed with Lyon's integral modeling approach for this Reynolds number.

Acknowledgements—The present research was supported by National Science Foundation Grant GK-4003. H. G. Buhr, T. W. Flaherty, R. N. Houze, A. K. Kudva, and R. V. G. Menon provided invaluable assistance during the various phases of this work.

REFERENCES

1. R. C. Martinelli, Heat transfer to molten metals, *Trans. Am.Soc.Mech.Engrs* **69**, 947 (1947).
2. O. E. Dwyer, Eddy transport in liquid-metal heat transfer, *A.I.Ch.E. Jl* **9**, 261–268 (1963).
3. R. Jenkins, Variations of the eddy conductivity with Prandtl modulus and its use in the prediction of turbulent heat transfer coefficients, Heat Transfer and Fluid Mechanics Institute, Preprints of Papers, 147, Stanford University Press (1951).
4. H. W. Kropholler and A. D. Carr, The prediction of heat and mass transfer coefficients for turbulent flow in pipe at all values of the Prandtl or Schmidt number, *Int. J. Heat Mass Transfer* **5**, 1195–1205 (1962).
5. J. O. Hinze, *Turbulence*. McGraw-Hill, New York (1959).
6. L. E. Hochreiter, Turbulent structure of isothermal and nonisothermal liquid metal pipe flow, Ph.D. Thesis, Purdue University (1971).
7. S. P. S. Arya, Structure of stably stratified turbulent boundary layer, Ph.D. Thesis, Colorado State University (1968).
8. W. E. Burchill, Statistical properties of velocity and temperature in isothermal and nonisothermal turbulent pipe flow, Ph.D. Thesis, University of Illinois (1970).
9. M. F. Cohen, Turbulence in water during pipe flow, M. S. Thesis, Ohio State University (1962).
10. R. A. Gardner, Magneto-fluid-mechanic pipe flow in a traverse magnetic field with and without heat transfer, Ph.D. Thesis, Purdue University (1969).
11. G. K. Patterson, Turbulence measurements in polymer solutions using hot-film anemometry, Ph.D. Thesis, University of Missouri at Rolla (1966).
12. J. Laufer, The structure of turbulence in fully-developed pipe flow, NACA Report 1174 (1954).
13. R. P. Patel, Reynolds stresses in fully-developed turbulent flow down a circular pipe, Report No. 68-7, Mechanical Engineering Research Laboratories, McGill University (1968).
14. A. K. Kudva and A. Sesonske, Structure of turbulent velocity and temperature fields in ethylene glycol pipe flow pipe at low Reynolds number, *Int. J. Heat Mass Transfer* **15**, 27 (1972).
15. V. A. Sandborn, Experimental evaluation of momentum terms in turbulent pipe flow, NACA-TN-3266 (1955).
16. J. G. Knudsen and D. L. Katz, *Fluid Dynamics and Heat Transfer*. McGraw-Hill (1958).
17. J. C. Hill, The directional sensitivity of a hot-film anemometer in mercury, Ph.D. Thesis, University of Washington (1968).
18. R. L. Schlosser, The directional sensitivity of hot-film sensors, M. S. Thesis, Purdue University (1971).
19. L. E. Hochreiter and A. Sesonske, Thermal turbulence characteristics in sodium–potassium, *Int. J. Heat Mass Transfer* **12**, 114–118 (1969).
20. J. H. Rust and A. Sesonske, Turbulence temperature fluctuations in mercury and ethylene glycol in pipe flow, *Int. J. Heat Mass Transfer* **9**, 215–227 (1966).
21. K. Bremhorst and K. J. Bullock, spectral measurements of temperature and longitudinal velocity fluctuations in fully developed pipe flow, *Int. J. Heat Mass Transfer* **13**, 1313–1329 (1970).
22. M. A. Connor, Velocity, temperature and turbulence measurements in air under combined free and forced convection conditions, Ph.D. Thesis, Univ. of Cape Town, South Africa (1971).
23. J. K. Jacoby and A. Sesonske, Free convection distortion and eddy diffusivity effects in turbulent mercury heat transfer, *Trans. Am. Nucl. Soc.* **15**, 408 (1972).
24. E. A. Horsten, Combined free and forced convection in turbulent flow of mercury, Ph.D. Thesis, Univ. of Cape Town, South Africa (1971).
25. J. R. Travis, H. O. Buhr and A. Sesonske, A model for velocity and eddy diffusivity distributions in fully turbulent pipe flow, *Can. J. Chem. Engng* **49**, 14 (1971).
26. R. N. Lyon, *Chem. Engng Prog.* **47**, 75–79 (1951).

STRUCTURE TURBULENTE DE L'ECOULEMENT ISOTHERME OU NON D'UN METAL LIQUIDE DANS UN TUBE

Résumé—On étudie à l'aide d'un anémomètre à film chaud l'écoulement du mercure dans un tube, avec ou sans transfert de chaleur, à un nombre de Reynolds de 50.000. On réalise une section de mesure chauffée à un flux constant de 12044 W/m^2 pour un diamètre de 3,64 cm.

Les mesures de fluctuation de vitesse axiale dans l'écoulement isotherme sont faites avec des jauges à film chaud à éléments simples ou croisés. L'accord général avec les résultats correspondant au cas de l'air indique que l'écoulement turbulent du mercure est semblable à celui des autres fluides. La production et la dissipation de l'énergie cinétique turbulente sont calculées à partir des résultats des mesures et s'accordent avec les résultats de Laufer pour l'air.

Les fluctuations de température mesurées avec l'anémomètre à film chaud utilisé en résistance thermométrique, s'accordent avec les résultats des autres techniques de mesure.

Le flux thermique axial turbulent ($\rho c_p \overline{u'_x \theta'}$) et le flux thermique radial ($\rho c_p \overline{u'_r \theta'}$) sont mesurés a l'aide des sondes à film chaud —simples et croisées—avec une méthode de Kovasznay modifiée pour séparer les sensibilités à la température et à la vitesse. La combinaison de la sensibilité assez faible à la vitesse et de la grande sensibilité à la température, et l'existence d'une convection naturelle axiale surajoutée ont pour résultat une incertitude sur $\overline{u'_x \theta'}$. Les valeurs mesurées de $\overline{u'_r \theta'}$ sont inhabituellement élevées dans la région de la paroi mais les transports convectif et conductif sont presque égaux.

TURBULENTE STRUKTUR ISOTHERMER UND NICHTISOTHERMER ROHRSTRÖMUNG VON FLÜSSIG- METALL

Zusammenfassung—Die Struktur einer voll entwickelten Quecksilber-Rohrströmung, mit und ohne Wärmeübertragung, wurde bei Reynolds-Zahlen von 50000 untersucht mit Hilfe eines Heissfilmanemo-

meters. Quermessungen wurden durchgeführt in einem senkrechten, beheizten Testabschnitt von 36,4 mm Durchmesser bei einem konstanten Wärmestrom durch die Wand von 1,2 W/cm^2. Die Messungen der Azialgeschwindigkeit der turbulenten isothermen Rohr-Strömung wurden sowohl mit einer x- Sonde als auch mit Einzelsonden gemacht.

Die Radialgeschwindigkeit und die Schubspannung der turbulenten Strömung wurde ebenfalls mit einer x- Sonde gemessen. Allgemein stimmen die Geschwindigkeitsmessungen mit Messungen in Luft überein und zeigen, dass die Struktur der turbulenten Quecksilberströmung mit der anderer Flüssigkeiten vergleichbar ist. Entstehung und Auflösung der turbulenten kinetischen Energie wurden aus Einzelsonden und x- Sonden Daten berechnet und stimmen gut mit den Daten für Luft nach Laufer überein. Die Temperatur der turbulenten Strömung, gemessen mit einem Heissfilmanemometer und einem Widerstandsthermometer, stimmt mit den Ergebnissen aus anderen Messmethoden gut überein. Der turbulente axiale Wärmestrom, $\rho c_p \overline{u^1 \theta^1}$ und der turbulente radiale Wärmestrom, $\rho c_p \overline{u_r^1 \theta^1}$ wurde ebenfalls mit Einzel- und x- Heissfilmsonden gemessen unter Benützung einer modifizierten Kovasznay —Methode, um die Temperatur—und Geschwindigkeitsempfindlichkeiten zu trennen.

Die Kombination einer geringen Geschwindigkeits- mit einer grossen Temperaturempfindlichkeit und die überlagerung der axialen Konvektion liefern streuende Werte für $\overline{u_x' \theta'}$. Die gemessenen Werte für $\overline{u_r' \theta'}$ wurden in Wandnähe ungewöhnlich gross, zeigen aber, dass Konvektions- und Leitungsanteil in der Mitte des turbulenten Gebiets fast gleich sind.

ТУРБУЛЕНТНАЯ СТРУКТУРА ИЗОТЕРМИЧЕСКОГО И НЕИЗОТЕРМИЧЕСКОГО ТЕЧЕНИЙ ЖИДКОГО МЕТАЛЛА В ТРУБЕ

Аннотация—С помощью пленочного термоанемометра исследовалась структура полностью развитого течения ртути в трубе при наличии и отсутствии переноса тепла и числе Рейнольдса, равном 50 000. Измерения проводились попкрек вертикального нагреваемого опытного участка диаметром 1,434 дюйма при постоянном тепловом потоке на стенке, равном 3820 БТЕ/час фут^2.

Измерения турбулентных колебаний скорости вдоль оси при изотермическом течении в трубе производились с помощью пленочного зонда с х-датчиком, а также зондом с единичным датчиком. С помощью х-датчика измерялись также интенсивность радиальных турбулентных колебаний скорости и турбулентное касательное напряжение. Общее совпадение результатов с соответствующими измерениями, выполненными в воздухе, указывает на то, что турбулентная структура скорости течения ртути аналогична течениям других жидкостей. Величина и диссипация турбулентной кинетической энергии рассчитывались по данным единичного датчика и х-датчика. Найдено, что результаты близко согласуются с данными Лауфера для воздуха.

Найдено, что турбулентные колебания температуры, измеренные с помощью пленочного термоанемометра, используемого в качестве термометра сопротивления, согласуются с результатами, полученными другими измерительными методами.

Турбулентный тепловой поток вдоль оси $\rho c_p \overline{u' \theta'}$ и турбулентный радиальный тепловой поток $\rho c_p \overline{u_r' \theta'}$ также измерялись термозондами с единичным датчиком и х-датчиком модифицированным методом Коважного для раздельного определения температуры и скорости. В результате относительно слабой чувствительности к скорости и большой чувствительности к температуре и наложения аксиальной свободной конвекции получены неопределенные значения $\overline{u_x' \theta'}$. При измерении получены необычно большие значения $\overline{u_r' \theta'}$ в пристеночной области, которые указывают на то, что в зоне турбулентного ядра конвективный и кондуктивный перенос почти одинаковы.